Article ID: 1671-3664(2007)04-0401-08 **DOI**: 10.1007/s11803-007-0787-2

Performance of a base isolator with shape memory alloy bars

Fabio Casciati†, Lucia Faravelli† and Karim Hamdaoui‡

Dept. of Structural Mechanics, University of Pavia, Pavia, Italy

Abstract: A new and innovative base isolation device is introduced in this paper based on extensive research carried out by the authors and their co-workers. A prototype of the device was built and experimentally tested on the shaking table. The new base isolation device consists of two disks, one vertical cylinder with an upper enlargement sustained by three horizontal cantilevers, and at least three inclined shape memory alloy (SMA) bars. The role of the SMA bars is to limit the relative motion between the base and the superstructure, to dissipate energy by their super-elastic constitutive law and to guarantee the re-centring of the device. To verify the expected performance, a prototype was built and tested under sinusoidal waves of displacement of increasing frequency with different amplitudes. It is shown that the main feature of the proposed base isolation device is that for cyclic loading, the super-elastic behavior of the alloy results in wide load-displacement loops, where a large amount of energy is dissipated.

Keywords: base isolator; dynamic excitation; energy dissipation; shape memory alloy; shaking table test

1 Introduction

Smart base isolated buildings (Skinner *et al*., 1993; Soong and Dargush, 1997; Nagarajaiah, 2007) have been studied for years throughout the world, both for near- and far-field earthquakes, due to their affordability in terms of production and maintenance.

The concept of a base isolator can be simply implemented in a sliding support. Many devices are available on the market, ranging from very small micro-sizes devices to the large devices used in civil engineering applications. In engineering applications, Western manufacturers primarily focus on rubber base isolators; the technology involved is simple and well understood (Casciati, 2003). Indeed, such industries were also established in other countries such as Armenia and India as a result of special international programs of cooperation. The devices from Far East manufacturers, in particular from Japan, are more sophisticated and better articulated. These include ball bearing isolators (Tanigawa *et al*., 2004; Hata and Ogura, 2004), which follow a concept originally suggested in Russia many years ago (Eisemberg *et al*., 1996), together with high technology "crossed linear bearing isolators" (Hata and Ogura, 2004; Kubo and Suzuki, 2004) that resist both tensile and compressive forces. Taisei Corp. (2004) also offers a rigid sliding bearing made of a Poly-Tetra-Fluoro-Ethylene (PTFE) plate. However, none of these devices can satisfy all the criteria required for use in civil engineering applications. These criteria include:

(i) Sliding should not occur under low intensity excitations to counteract static or semi-static actions;

(ii) Reparability should be provided by replacing either the entire device or its single components;

(iii) Working temperature window should satisfactorily account for day-night and winter-summer variations;

(iv) A policy should be adopted to manage very large displacements;

(v) A re-centering strategy should be incorporated;

(vi) Energy should be dissipated by a parallel damper or another added component.

Item (v) is the main drawback of existing friction devices, while item (iii) makes the use of isolators built by superimposing several sets of disks in steel and rubber dangerous. Item (vi) was achieved in the past by inserting a lead inclusion (in conflict with Item (v)), but lead is no longer used in technological application because it is poisonous. Shape memory alloys (SMAs) have been investigated (Tahiri *et al*., 1994) as a replacement for lead.

This paper introduces a base isolator with a new architecture. The new isolator results from an assemblage of several components, each with its own function. The architecture of this isolator is described first, followed by a description of a prototype device. Finally, the test

Correspondence to: Fabio Casciati, Dept. of Structural Mechanics, University of Pavia, Pavia, Italy
Tel: +39 0382 985458
E-mail: fabio@dipmec.unipv.it
†Professor; ‡PhD Student

Supported by: Italian National Research Council (CNR) Under Grant No CU07.00016.ST/97

Received November 10, 2007; **Accepted** November 16, 2007

program is presented, which shows that the new base isolator meets expected performance objectives.

2 Geometry of the device

The base isolation device proposed in this paper is composed of two disks, one vertical cylinder with an upper enlargement sustained by three horizontal cantilevers, and at least three inclined SMA bars. The following geometric parameters characterize the assemblage as illustrated in Fig. 1:

B = diameter of the bottom disk of thickness s_1;

D = diameter of the top disk of thickness s_2;

b = diameter of the vertical cylinder;

ϕ = diameter of the SMA bar;

l = length of the cantilever measured from the axis of the cylinder;

L = length of projection of the cantilevers; a lateral view would provide $L = 1.5\ l$; a front view would provide $L = 3^{1/2}\ l$;

h = distance between the two horizontal disks;

d_1 = diameter of the inner circle on the bottom disk where the bars are placed;

d_2 = diameter of the inner circle on the top disk where the bars are placed.

Note that the bars are not only joining points on circles of different diameters, but the points on the top circle are rotated 180°.

The disks and cylinder can be made of steel, aluminium or nylon. The SMA (Auricchio *et al*., 2001) adopted in this paper is the copper-aluminium-beryllium (Cu-Al-Be) alloy studied in depth by the authors and their co-workers (Casciati and Faravelli, 2004, 2007; Casciati and van Eijk, 2008). Its important features are its austenite transformation finish temperature, which is lower than 0°C, and its ability to preserve the shape of its hysteretic super-elastic cycles up to temperatures much higher than 100°C.

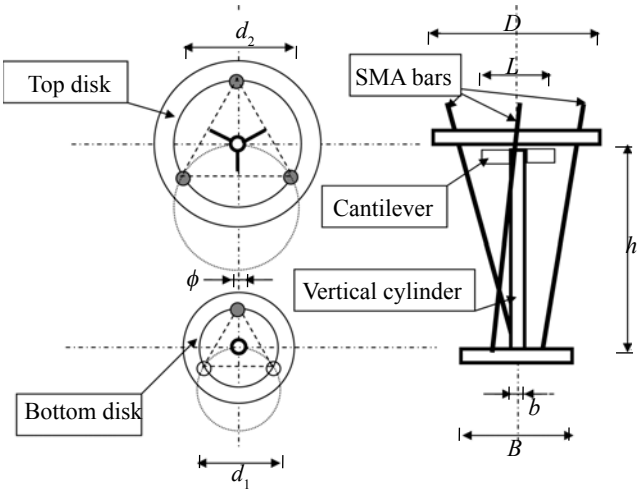

Fig. 1 Geometry of the proposed device. The view on the left is from the top on the bottom disk and from the bottom on the top disk

A similar device, with the alloy bar fixed both at the bottom and top disks, was investigated in depth numerically by the authors and their co-workers (Casciati *et al*., 2006; Casciati, Faravelli and Hamdaoui, 2007 a, b, c and d). A general purpose finite element code offering a super-elastic constitutive law was adopted for this analysis. Unfortunately, the use of this material routine was restricted to plane and solid finite elements. Therefore, hexagon elements were adopted to discretize each SMA bar, which made the computational effort very difficult. In addition, the routine did not account for the actual austenite-martensite transformations and was inadequate in managing the different responses of the device to tension and compression. As a result, the numerical response was not consistent with the experimental evidence. The first laboratory tests were carried out as reported in Casciati and Hamdaoui (2007) and some noteworthy observations are as follows:

(a) A device made only of inclined SMA bars, without the presence of the vertical cylinder, could also be realized, but the vertical sustainable load would result strongly reduced. Moreover, the expected benefit of adopting SMA bars is undermined by the large amount of resources required to support the vertical loads;

(b) Bars fixed at the top disk, as modelled in the numerical studies, result into rotations of the top disk around the vertical axis, as well as in its rolling due to the large displacement geometric effect; this suggests that sliding bars must be much longer than the length required at rest;

(c) When the bars are fixed at both ends and also support the vertical loads, the bar inclination on the vertical axis was optimized. The optimum value was shown to be 30° and this design value is adopted in the prototype built and tested in this paper;

The fatigue performance of the bars (as investigated in Casciati *et al*., 2007) was very satisfactory. Moreover, the bars were fully recovered after cycles of loading and unloading using suitable thermal treatments (Casciati, 2007).

3 Prototype test and system identification

Figure 2 provides the details of the prototype base isolator (made by two aluminium disks, three SMA bars and one vertical cylinder). The upper aluminium disk (diameter D = 25 cm and thickness s_1 = 2 cm) serves as a superimposed tray: the system to be isolated will be mounted on it. The three SMA bars are a diameter of ϕ =3.5 mm and $\geq$20 cm long. The bars, inclined 30° on the vertical axis z, were free to move at the top end but fixed at the bottom to the lower aluminium disk (diameter B = 15 cm and thickness s_2 = 1.5 cm).

The role of the vertical shaft, with a diameter of b = 2.6 cm (4 cm in the upper part) and a height of h = 16 cm, placed at the center of the tested prototype, is to

absorb the vertical load of the structure to be isolated. Consequently, only the horizontal action engages the inclined SMA bars. Note that between the head of the cylinder and the top aluminium disk, a Teflon layer is added to facilitate the sliding. To complete the prototype geometry, the diameter of the inner circle on the bottom disk where the bars are placed, is $d_1 = 3.8$ cm while the diameter of the inner circle on the top disk where the bars are placed, is $d_2 = 18.2$ cm.

As shown in Fig. 3, the device bottom disk is fixed to the shaking table in the Vibration Laboratory at the University of Pavia. A mass of 31 kg is placed on its top. The two accelerometers which were used to capture the accelerations are also shown on the shaking table and on the top of the device.

During the tests, an eight-channel acquisition system received the signals measured by four sensors. Two are mono-axial accelerometer FBA-11 EP-sensors, made by Kinemetrics, and are mounted on the table and top mass, respectively. The other two channels use two Wenglor non-contact displacement laser sensors (located on a mass outside the table) for measuring the displacements of the bottom and top disks.

The sensors are linked to the acquisition system through a junction box, which provides power to the sensors and, at the same time, receives the signals from them. An anti-aliasing filter at 10 Hz is performed by the acquisition device, before the A/D (analog/digital converter) transfers the signals to the PC for storage.

Standard shaking table tests were carried out to evaluate the dynamic characteristics of the structural model. Long records of the response were collected when the model was excited at the base by acceleration white-noise. The shaking table was driven by a displacement time history of long duration, i.e., 5 minutes, whose corresponding acceleration time history fits a white-noise spectrum in the range from 0 to 20 Hz. The intensity was modified by either scaling the integrated displacement and forwarding it to the shaking table as reference input, or by modifying the shaker span.

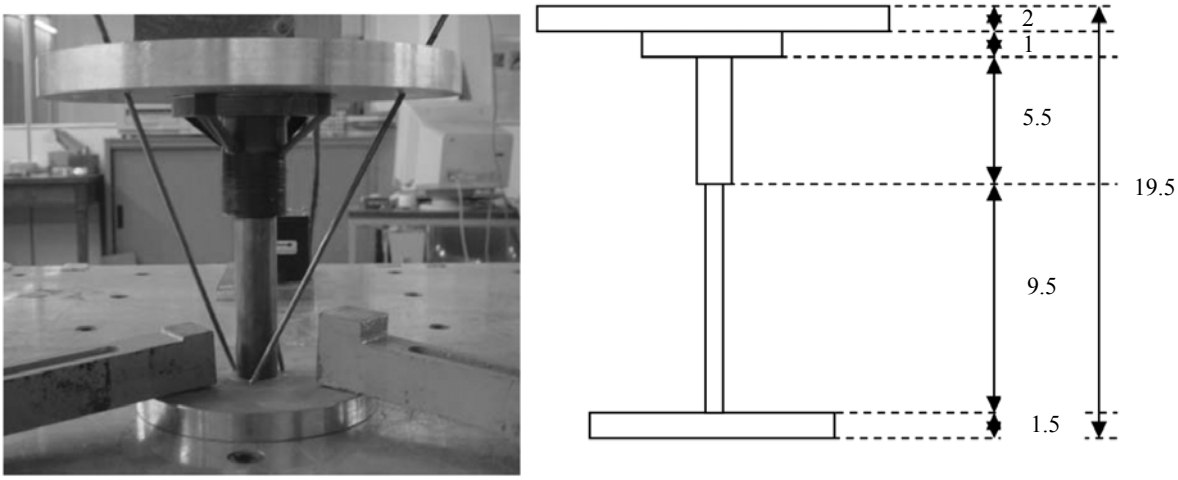

Fig. 2 Prototype of base isolator (dimensions are shown in cm)

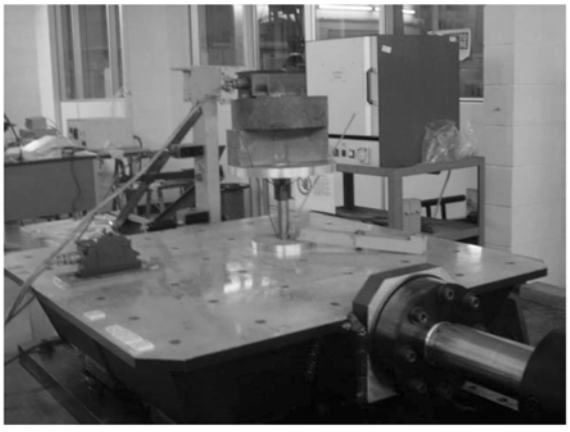

Fig. 3 Prototype device fixed on the shaking table

However, the intrinsic nature of the device is nonlinear. The global stiffness primarily depends on the excitation intensity (due to the SMA constitutive law), while the device response is significantly different when above or below the force threshold, which results from friction and the SMA bar contrast. In order to identify the last force, it was decided to perform the tests by sinusoidal waves of displacement $u(t)$ of increasing frequency f for given span U of the shaking table piston:

$$u(t) = U \sin (2\pi f t) \tag{1}$$

where t denotes the time. The prototype device was tested for three sets of shaking span amplitudes: 10 mm, 12.5 mm and 15 mm. For each test, several sequences of

sinusoidal excitations, with frequencies ranging from 1 to 4 Hz, were generated.

The sensor readings provide the measured time histories of the bottom and top displacements, $u_b(t)$ and $u_t(t)$, and accelerations, $a_b(t)$ and $a_t(t)$, respectively. They allow the relative displacement between the top and bottom disks to be estimated as follows:

$$\Delta u(t) = u_t(t) - u_b(t) \tag{2}$$

and the inertia force of the top mass:

$$F = m\, a_t(t) \tag{3}$$

The limit force F_y is defined as the value of the force in Eq. (3) for which there was a discontinuity in Eq.(2). Note that the device does not have a symmetrical axis,, but its geometry is based on equilateral triangles and should provide a type of isotropic response. The asymmetry in the values of F_y in the two directions indicates a deviation from this isotropy. The pairs (π^{2f^2U}, F_y) revealed by the experiments are shown in Fig.4. Note that the force is nearly constant (around 62N, accepting a flat friction coefficient of 0.2, the mass being 31 kg!). This means that the top acceleration at sliding is nearly the same, while the base acceleration decreases as the excitation intensity increases. In other words, the acceleration amplification factor (calculated as the ratio between the maximum absolute accelerations detected at the top over the bottom) varies with the excitation frequency even before the sliding.

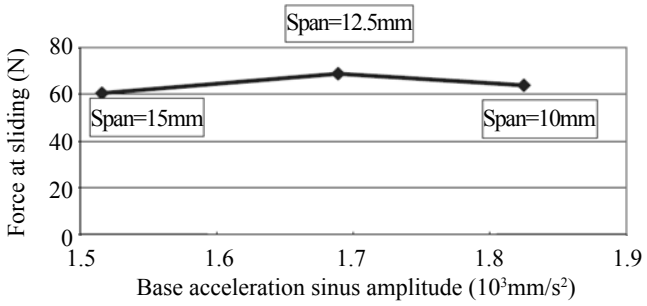

Fig. 4 Pairs ($4\pi^2 f^2 U$, F_y) revealed during the experimental program

In particular, the amplification factors of displacement and acceleration are different due to the nonlinear characteristics of the system. They are summarized in Fig.5 for the three span values adopted in the experimental program. The discontinuities in Fig. 5(a) are due to the sensor resolution. The values shown in Fig. 5(b), higher than the corresponding values in Fig.5(a), are due to the fact that the device stiffness increases to avoid large displacements, which results in values of the top acceleration being comparable with those at the base (see Section 4 for a more detailed explanation).

The sliding threshold satisfies the first requirement listed in the introduction; that is, the sliding should not occur under low intensity excitations to counteract static or semi-static actions. Reparability (Item ii) is satisfied by the simple assemblage scheme of the device, while the suitability of the working temperature (Item iii) is achieved by the specific selection of the shape memory alloy.

Requirements (iv) – (vi) are discussed in Section 4, based on the experimental results first.

4 Test details and hysteresis loops

As mentioned in the previous section, hysteresis is pursued in the relationship between the force at the top of the device (estimated from the measured top acceleration) and the relative displacement (achieved as the difference between the laser sensors readings). The measurements were collected for three different values of vibration intensity, fixed by assigning the span of the shaking table piston: 10, 12.5 and 15 mm. Each excitation time history is sinusoidal of increasing frequency.

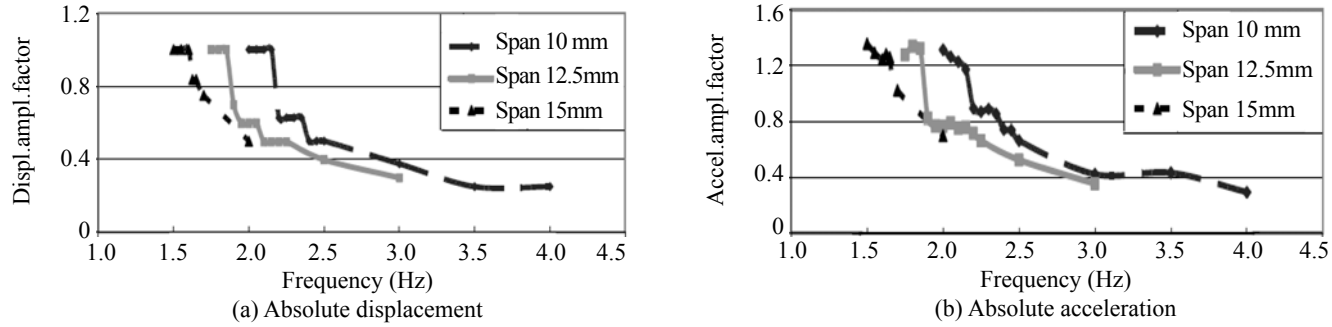

Fig. 5 Amplification factors

4.1 Test with amplitude of 10 mm

The test was started with an initial frequency of 2

Hz; it was then slowly increased up to 4 Hz. Signals were recorded for the following intermediate values: 2.00, 2.05, 2.10, 2.15, 2.20, 2.25, 2.30, 2.35, 2.40, 2.45, 2.50, 3.00, 3.50, 4.00 Hz.

Initially no significant relative displacement between the top and the bottom disk was detected. In other words, the top force was lower than the friction force between the upper side of the vertical cylinder and the aluminium plate. At the frequency of 2.20 Hz, the top plate moves independently of the bottom disk; the hysteretic behavior is emphasized as seen in Figs. 6 and 7. Similar plots could be reported for all the tests excited at greater values of the frequency.

In Fig. 6, from the rest to the stationary cycles, the force varies first, for negligible relative displacements, below the negative threshold. Then, the threshold is achieved and the graph follows a few irregular loops until the motion stabilizes along the stationary cycles. Each cycle shows low forces at zero displacements and peak values of nearly 40 N (and -40 N) for large positive relative displacements (15 mm) and large negative values (-15 mm).

In Fig. 7, the stationary response is perturbed when the excitation is switched off; note the ability of the device to re-center itself, with force and displacement returning to the initial rest position. To understand the response in more detail, the acceleration signal was filtered by a band-pass between 0.5 and 4 Hz. The plot of the filtered force is shown in Fig. 8, where contributions to the global motion in Figs. 6 and 7 of higher frequency modes, which are now suppressed, are seen. The filtered time history shows a constant time delay of the peaks with respect to the peaks achieved by the base acceleration.

As the frequency increases, two stages occur: first, the top acceleration increases, as does the force; then the base isolation actually occurs. In stage 1, an increase of the maximum relative displacement would be expected, but as shown in Fig. 9 for a frequency of 2.35 Hz, the device reacts by increasing the stiffness, which constraints the maximum displacement to remain at 15 mm. However, the corresponding acceleration peak does not de-amplify.

Note that the device globally reacts in a way quite similar to any elastomeric material, showing an initial stiffness at low strain, a large flexibility at a strain of 100% and finally a large stiffness, which prevents very large displacements.

When the frequency is further increased, a full isolation is reached (stage 2). The hysteresis assumes the shape in Fig. 10, drawn for a frequency of 4 Hz, and the maximum value of the relative displacement is lower than the values in Figs. 6 to 9.

4.2 Test with amplitude of 12.5 mm

In this test, the oscillation amplitude is increased by adopting a span value of 12.5 mm. Here, the initial frequency is 1.75 Hz, and is slowly increased up to 3 Hz (1.75, 1.80, 1.85, 1.90, 1.95, 2.00, 2.05, 2.10, 2.15, 2.20, 2.25, 2.50, 3.00 Hz). The first hysteresis loop was detected for the frequency of 1.90 Hz, i.e., the horizontal force exceeded the friction force between the upper part of the vertical shaft and the aluminium plate. Figures 11 and 12 plot this situation, while Fig. 13 provides the graph obtained for 3 Hz. Note that the maximum relative displacement is now 20 mm.

4.3 Test with amplitude of 15 mm

In the test with the largest span value of 15 mm, the initial frequency was 1.50 Hz, and gradually increased up to 2 Hz (1.50, 1.55, 1.60, 1.625, 1.65, 1.70, 2.00Hz). The friction force threshold was achieved for a frequency of 1.625 Hz. Figures 14 and 15 illustrate this situation. Note that while the displacement amplification factor is small, the one associated with the acceleration is large. Indeed, large accelerations are required to prevent large

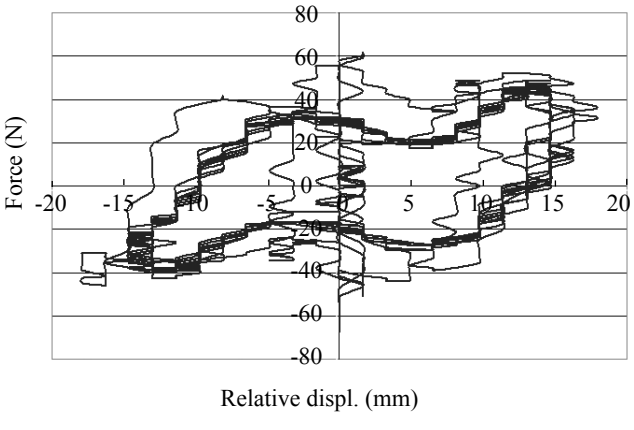

Fig. 6 Top force vs. relative displacement: amplitude 10mm, frequency 2.20Hz. From the rest to the stationary response: duration 8 s

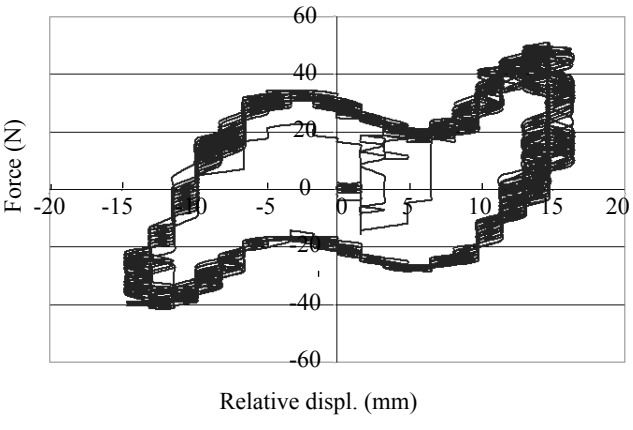

Fig. 7 Top force vs. relative displacement: amplitude 10mm, frequency 2.20Hz. From the stationary response to rest: emphasis on the re-centring ability

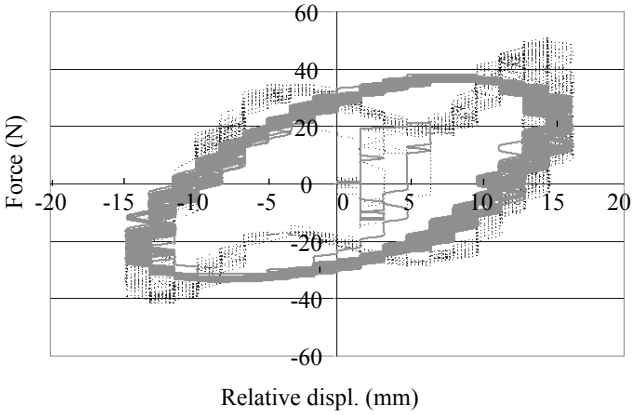

Fig. 8 Top force vs. relative displacement: amplitude 10mm, frequency 2.20Hz. From the stationary motion to rest. Actual signal in dotted line; filtered signal in solid line

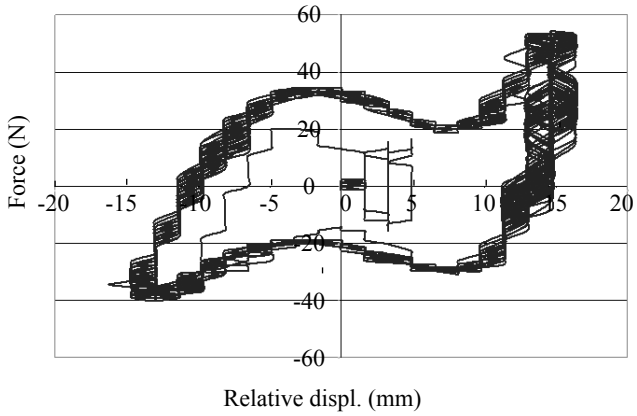

Fig. 9 Top force vs. relative displacement: amplitude 10mm, frequency 2.35 Hz. From the stationary response to rest: emphasis on the way the maximum displacement is limited by increasing the force value

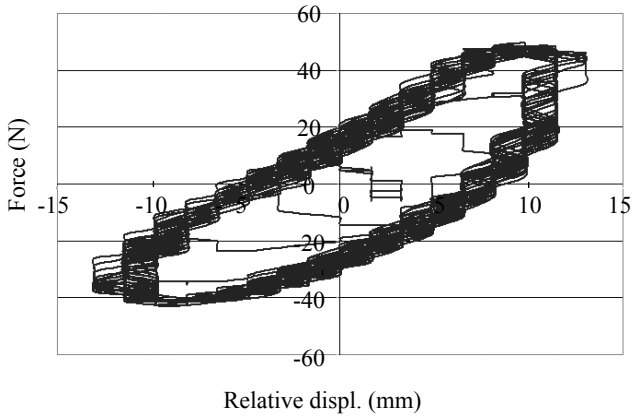

Fig. 10 Top force vs. relative displacement: amplitude 10mm, frequency 4 Hz. From the stationary response to rest: emphasis on the reduced value of the maximum displacement

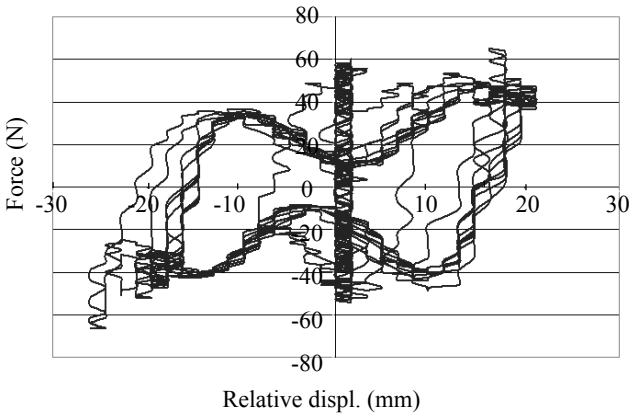

Fig. 11 Top force vs. relative displacement: amplitude 12.5mm, frequency 1.90Hz. From the rest to the stationary response: duration 12 s

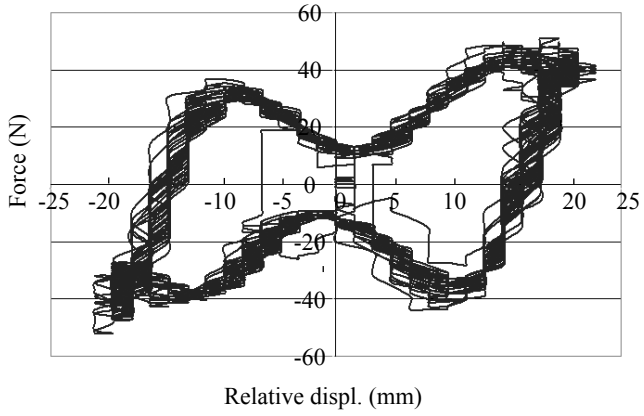

Fig. 12 Top force vs. relative displacement: amplitude 12.5mm, frequency 1.90Hz. From the stationary response to rest: emphasis on the re-centering ability

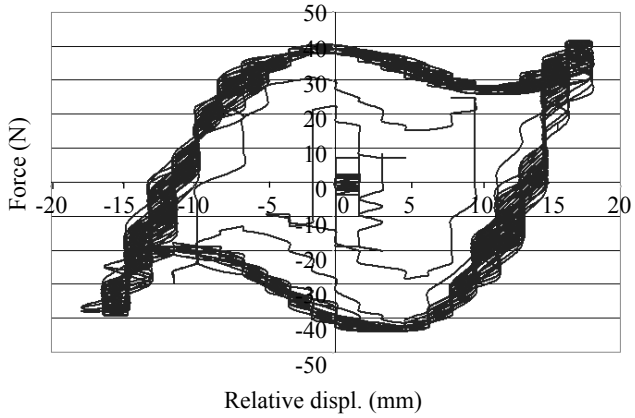

Fig. 13 Top force vs. relative displacement: amplitude 12.5 mm, frequency 3 Hz. From the stationary response to rest: emphasis on the reduced value of the maximum displacement

displacements. The value of the maximum relative displacement (25 mm) also increased.

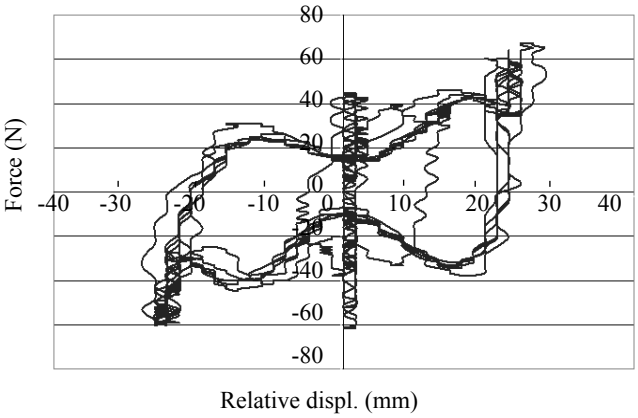

Fig. 14 Top force vs. relative displacement: amplitude 15mm, frequency 1.625Hz. From the rest to the stationary response: duration 12 s

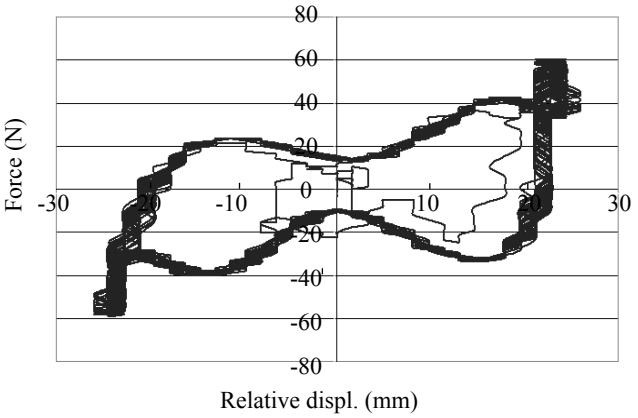

Fig. 15 Top force vs. relative displacement: amplitude 15mm, frequency 1.625 Hz. From the stationary response to rest: emphasis on the re-centring ability

5 Conclusions

This paper describes a new and innovative base isolator in which a sliding system is coupled with inclined bars in shape memory alloy in its austenite phase. These bars have four functions:

(i) to provide stiffness against low intensity excitations;

(ii) to contrast very large displacements;

(iii) to re-center the device;

(iv) to dissipate energy during the motion.

Based on experimental observations carried out on a prototype, the main feature is that for cyclic loading, the super-elastic behavior of the alloy results in wide load-displacement loops, where a large amount of energy is dissipated. These loops become smaller and smaller as the excitation intensity decays, resulting in the device re-centring.

The following research topics should be investigated in more detail:

(1) Dynamic comparison: the behavior of the sliding system without SMA bars should be recorded during experimental tests where the excitation is increased up to the collapse of the top disk;

(2) Performance characterization: the ratio between the diameters of the top disk over the bottom disk should be optimized;

(3) Geometric design: the bar inclination should be optimized; it is likely that this depends on the device height and the above diameter ratio;

(4) Numerical modelling: the difficulties met in achieving a satisfactory modelling of the shape memory alloy mainly depend on the adoption of solid hexagonal finite elements; refinements of the mesh only where absolutely necessary or the development of user-subroutines that account for specific exploitation of the alloy should be investigated;

(5) Carrying capacity: while waiting for a reliable numerical model, the existing device should be tested with different masses to identify the vertical carrying capacity to allow a large enough margin to undergo horizontal motions;

(6) Design scaling: until a reliable numerical model is developed, prototypes of different sizes should be constructed to collect preliminary information on the way a larger device could be developed;

(7) Alloy alternative: despite being more expensive, nickel-titanium (Ni-Ti) alloys are often used in engineering applications; therefore prototypes using this different shape memory alloy should also be tested in different environment conditions.

Acknowledgements

This paper resulted from a research effort that originated under the umbrella of the FP6 European Union project WIND-CHIME. The experimental research was funded by the Italian National Research Council (CNR), within the national program for which Prof. A. Di Tommaso, of the University of Venice, Italy, is serving as topic coordinator. Data processing was supported by an athenaeum research contribution from the University of Pavia to the second author.

References

Auricchio F, Faravelli L, Magonette G and Torra V (2001), *Shape Memory Alloys: Advances in Modelling and Applications*, Barcelona: CIMNE.

Casciati F (2003), ed., *Proceedings Third International Conference on Structural Control,* Como: John Wiley & Sons.

Casciati F, Casciati S and Faravelli L (2007), "Fatigue Characterization of a Cu-based Shape Memory Alloy," *Proceedings of the Estonian Academy of Sciences – Physics Mathematics*, **56**(2): 207-217.

Casciati F and van Eijk C (2008), "Mechanical Properties and Microstructure Characterization of CuAlBe Shape Memory Alloys for Vibration Mitigation**,**" Accepted for Publication in *Smart Structures & Systems.*

Casciati F and Faravelli L (2004), "Experimental Characterisation of a Cu-based Shape Memory Alloy Toward Its Exploitation in Passive Control Devices," *Journal de Physique IV*, **115**: 299-306.

Casciati S and Faravelli L (2007), "Structural Components in Shape Memory Alloy for Localized Energy Dissipation," Accepted for Publication in *Computer & Structures*.

Casciati F, Faravelli L and Hamdaoui K (2006), "Reliability Study for a New Concept of Base Isolator," *Proceedings Fifth International Conference on Computational Stochastic Mechanics*, June 20-23. Rhodes, Greece, pp. 163-168.

Casciati F, Faravelli L and Hamdaoui K (2007a), "A Base Isolation Device with Bars in Shape Memory Alloys," *Proceedings First International Conference on Self Healing Materials*, Amsterdam, The Netherlands.

Casciati F, Faravelli L and Hamdaoui K (2007b), "Shape Memory Alloy Bars Assembled in a Base Isolator," *Proceeding of the ANCER Conference,* Hong Kong.

Casciati F, Faravelli L and Hamdaoui K (2007c), "Performance-based Design of a Shape Memory Alloy Base Isolator," *Proceeding of the 10th International Conference on Applications of Statistics and Probability in Civil Engineering*, Tokyo, Japan.

Casciati F, Faravelli L and Hamdaoui K (2007d), "Numerical Modelling of a Shape Memory Alloy Base Isolator," *Proceedings of 3rd International Conference on Structural Engineering, Mechanics and Computation*, Cape Town, South Africa.

Casciati F and Hamdaoui K (2007), "Modelling the Uncertainty in the Response of a Base Isolator," Submitted for Publication in *Probabilistic Engineering Mechanics.*

Casciati S (2007), "Thermal Treatment Optimization for Cu-based Shape Memory Alloys," *First International Conference on Self-Healing Materials*, Berlin: Springer Verlag.

Eisemberg JM, Smirnov VI and Stepanov AY (1996), "Seismoisolation and Structural Control Investigations and Applications in Russia," *Proceeding 1st European Conference on Structural Control*, Singapore: World Scientific Publishing, pp. 258-265.

Hata T and Ogura Y (2004), "Aseismic Devices Co: Development of Seismic Devices for Earthquake Protection," *Proceedings of International Symposium for Smart Structures Technologies and Earthquake Engineering (SE04)*, Separate Technology Volume, Osaka: Bandoh Printing & Package Ltd., Japan, pp. 5-9.

Kubo A and Suzuki J (2004), "Mitsubishi Heavy Industries: Vibration Control and Earthquake Isolation Systems," *Proceedings of International Symposium for Smart Structures Technologies and Earthquake Engineering (SE04)*, Separate Technology Volume, Osaka: Bandoh Printing & Package Ltd., Japan, pp. 45-47.

Nagarajaiah S (guest ed.) (2006), "Structural Control Benchmark Problem: Phase I – Linear Smart Base Isolated Building Subjected to Near Fault Earthquakes," *Structural Control & Health Monitoring,* **13**(2-3): 571-822.

Skinner RI, Robinson WH, McVerry GH (1993), *An Introduction to Seismic Isolation*, Chichester: John Wiley & Sons.

Soong TT, Dargush GF (1997), *Passive Energy Dissipation Systems in Structural Engineering*, Chichester: John Wiley & Sons.

Tahiri VL, Patoor E and Eberhardt A (2004), "An Analysis of the Thermomechanical Behaviour of a Shape Memory Alloy/elastomer Composite," *Journal de Physique IV*, **115**: 195-203.

Taisei Corp (2004), "Sliding-type Base Isolation System," *Taisei Technical report*.

Tanigawa K, Yokoyama S, Yokobayashi Y (2004), "Sekisui House: Seismic Base-Isolated Detached House by Ball Bearing Isolators," *Proceedings of International Symposium for Smart Structures Technologies and Earthquake Engineering (SE04)*, Separate Technology Volume, Osaka: Bandoh Printing & Package Ltd., pp. 57-62.